


Article

Behavior of Fiber-Reinforced and Lime-Stabilized Clayey Soil in Triaxial Tests

Yixian Wang ¹, Panpan Guo ¹, Xian Li ^{1,*}, Hang Lin ^{2,*}, Yan Liu ³ and Haiping Yuan ¹¹ School of Civil Engineering, Hefei University of Technology, Hefei 230009, China;

wangyixian2012@hfut.edu.cn (Y.W.); 20113467@mail.hfut.edu.cn (P.G.); seapie@hfut.edu.cn (H.Y.)

² School of Resources and Safety Engineering, Central South University, Changsha, Hunan 410083, China³ State Key Laboratory of Explosion Science and Technology, Beijing Institute of Technology, Beijing 100081, China; bitliuyan@126.com

* Correspondence: 2011800022@hfut.edu.cn (X.L.); hanglin@csu.edu.cn (H.L.)

Received: 23 January 2019; Accepted: 26 February 2019; Published: 3 March 2019



Abstract: The beneficial role of combining fiber reinforcement with lime stabilization in altering soil behavior has been established in the literature. However, the coupling effect of their combination still remains unclear in terms of its magnitude and microscopic mechanism, especially for natural fibers with special microstructures. The objective of this study was to investigate the coupling effect of wheat straw fiber reinforcement and lime stabilization on the mechanical behavior of Hefei clayey soil. To achieve this, an experimental program including unconsolidated–undrained (UU) triaxial tests and SEM analysis was implemented. Static compaction test samples were prepared on untreated soil, fiber-reinforced soil, lime-stabilized soil, and lime-stabilized/fiber-reinforced soil at optimum moisture content with determining of the maximum dry density of the untreated soil. The lime was added in three different contents of 2%, 4%, and 6%, and 13 mm long wheat straw fiber slices with a cross section one-quarter that of the intact ones were mixed in at 0.2%, 0.4%, and 0.6% by dry weight of soil. Analysis of the derived results indicated that the addition of a small amount of wheat straw fibers into lime-stabilized soil improved the intensity of the strain-softening behavior associated with mere lime stabilization. The observed evidence that the shear strength increase brought by a combination of 0.4% fiber reinforcement and 4% lime stabilization was smaller than the summation of the shear strength increases brought by their presence alone in a sample demonstrated a coupling effect between fiber reinforcement and lime stabilization. This coupling effect was also detected in the comparisons of the secant modulus and failure pattern between the combined treatment and the individual treatments. These manifestations of the coupling effect were explained by a microscopic mechanism wherein the fiber reinforcing effect was made more effective by the ways in which lime chemically stabilized the soil and lime stabilization development was quickened by the water channels passing through the surfaces and honeycomb pores of the wheat straw fibers.

Keywords: coupling effect; fiber reinforcement; clayey; triaxial compression; combined treatment

1. Introduction

Civil infrastructure such as buildings, roadways, bridges, embankments, and dams is frequently built upon the usage of soil or rock materials. This kind of material has to be good enough in strength and deformation characteristics to ensure the safety and sustainability of civil infrastructure [1–7]. To capture and improve the behavior of geological materials, many studies have been carried out [8–17]. In many engineering applications, however, soils with unsatisfactory engineering properties are encountered [18,19], triggering the rapid development and wide application of soil improvement

techniques. These techniques fall into three main categories: physical techniques (e.g., vibration [20,21]), mechanical techniques [22], and chemical techniques (e.g., admixture stabilization [23]).

Reinforcing soil using randomly distributed fibers dates from more than 5000 years ago when plant roots and stems were used to reinforce building blocks. This technique still remains a hot research issue nowadays and its application fields are widening [24–27]. The advantages of mixing fibers into soil include increases in shear, compressive, and tensile strength [28–31]; a reduction in the swelling tendency of expansive soil [32–34]; reduced brittleness [35–38]; and so forth. Meanwhile, disadvantages like the slight reduction in initial stiffness with increasing fiber concentration observed by Michalowski and Čermák (2003) [38] are involved.

Soil stabilization with lime is a chemical technique that results in marked improvements in strength, compaction, and compressibility characteristics [39–43]; a reduction in expansive soil's swell percentage and swelling pressure [44,45]; and a decrease in plasticity [46–48], which can cause unfavorable brittle failure. To remedy this reduced plasticity, both synthetic and natural fibers have been added to lime-stabilized soil [49,50]. Although the beneficial role of a combination of lime stabilization and fiber reinforcement is an established concept [51–56], the coupling effect of them with regard to magnitude and microstructural mechanisms is not well understood, especially for natural fibers with special microstructures such as coir and wheat straw.

Wheat straw is an abundantly produced agricultural residue of which disposal by burning results in large amounts of air pollutants. An alternative way to dispose of wheat straw is utilization of it for soil reinforcement. The reinforcing effect of wheat straw fiber on the strength behavior of Shanghai clayey soil was reported in a study by Qu and Sun (2016) [57], and the feasibility of combining SH-treated (i.e., modified polyvinyl alcohol) wheat straw fiber reinforcement with lime stabilization to improve the properties of saline soil was verified by Li et al. (2012) [58]. They found that SH filled the pores distributed evenly on wheat straw's characteristic cross-sectional honeycomb pattern, thus improving the water resistance and tensile strength of the wheat straw fiber [59,60]. Nevertheless, the honeycomb pattern of untreated wheat straw fiber inevitably influences the coupling effect of wheat straw fiber reinforcement and lime stabilization. This influence has not been fully investigated [61,62].

This study is aimed at ascertaining the coupling effect of wheat straw fiber reinforcement and lime stabilization on the triaxial behavior of Hefei clayey soil. Based on results derived from a series of unconsolidated–undrained (UU) triaxial tests and scanning electron microscopy (SEM) analysis, the coupling effect is discussed and interpreted on a microcosmic scale.

2. Experimental Program

2.1. Materials

2.1.1. Hefei Clayey Soil

The soil used in this study was Hefei clay soil collected from a foundation for a metro station in Hefei, China. This kind of soil is brownish red in color and contains calcareous concretions within it. A high plastic limit and a slight expansive tendency differentiate Hefei clayey soil from other kinds of clayey soil. A series of laboratory experiments identified the basic properties of Hefei clayey soil, as presented in Table 1.

Table 1. Basic properties of Hefei clayey soil.

Property	Value
Specific gravity	2.75
Unit weight (g/cm ³)	1.56
Grain Size Analysis	
Sand (%)	15.4
Silt (%)	47.8
Clay (%)	36.8

Table 1. Cont.

Property	Value
Atterberg Limits	
Liquid limit (%)	57.1
Plastic limit (%)	19.7
Plasticity index	37.4
Compaction Study	
Optimum moisture content (%)	20.1
Maximum dry density (g/cm ³)	1.68
Shear Strength Parameters	
Cohesion (kPa)	64
Angle of internal friction (Deg)	21

2.1.2. Wheat Straw Fibers

The wheat straw fibers used in this study are presented in Figure 1. They were considered natural because they were not treated with any chemical additive such as the SH agent used by Li et al. (2012) [58]. The natural characteristics of wheat straw fibers were retained to achieve the objective of investigating how the coupling effect of wheat straw fiber reinforcement and lime stabilization was affected by the intact honeycomb pattern of wheat straw fibers. After having been dried in the sun, the wheat straw fibers were peeled and cut into slices with a complete cross section of one-quarter of the original and a length of 13 mm. This cross section and length of the wheat straw fiber slices were selected because they were optimal for mobilizing the reinforcing effect [58]. The physical and mechanical properties of the wheat straw fibers provided by the manufacturer are summarized in Table 2.

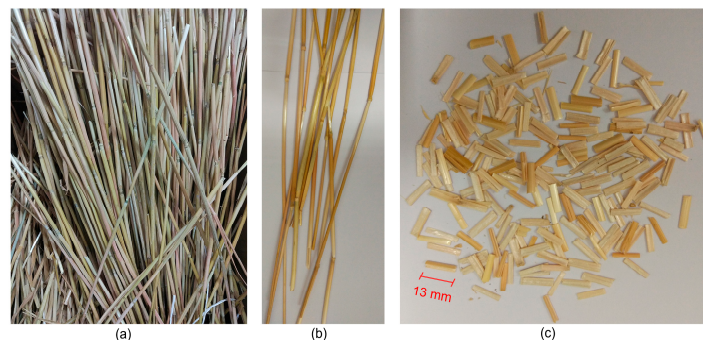


Figure 1. Photographs of wheat straw fibers: (a) natural wheat straw fibers, (b) peeled wheat straw fibers, and (c) wheat straw fibers trimmed to the required shape and length.

Table 2. Basic properties of wheat straw fibers.

Property	Value
Average diameter (mm)	3.1
Wall thickness (mm)	0.53
Ultimate tensile strength (N)	67
Ultimate elongation (%)	4.8
Bulk density (kg/m ³)	35.2
Water absorption capacity (20 °C, 28 days, %)	316
Chemical Composition	
Cellulose (%)	45.23
Hemicellulose (%)	34.02
Lignin (%)	16.90

2.1.3. Lime

Hydrated lime, in which calcium hydroxide predominates, was used in this study as the stabilization material. Calcium hydroxide accounts for approximately 90% of the lime weight. The other parts of the composition were calcium carbonate (1.8%), aluminum oxide (0.4%), ferric

oxide (0.3%), magnesium oxide (0.7%), silica (1.2%), and some impurities (5.9%). The impurities were removed by sieving (2 mm) before mixing the lime into the soil.

2.2. Sample Preparation

Four kinds of sample, differentiated according to the material added to soil, were considered in this study: (1) an untreated sample; (2) a lime-stabilized sample; (3) a fiber-reinforced sample; and (4) a lime-stabilized sample reinforced with fibers. In the samples containing lime, lime was added in three different content levels of 2%, 4%, and 6% as a percentage of the dry weight of the soil. For the samples into which wheat straw fibers were mixed, fiber contents of 0.2%, 0.4%, and 0.6% by dry weight of soil were chosen.

Cylindrical samples with a diameter of 39.1 mm and a height of 80 mm were prepared at the optimum moisture content and maximum dry density determined for untreated soil, no matter what material was added to the specimen. This operation was reasonable because the effect of the addition of these materials on the compaction characteristics of Hefei clayey soil was negligible according to the compaction testing results from this study. To achieve the desired maximum dry density, untreated soil and a mixture of soil and added material were poured progressively into a steel tube of inner diameter 39.1 mm and height 100 mm and then subjected to static compaction by a hydraulic jack.

The mixing of soil and fibers involved two steps. First, fibers were manually mixed into soil with approximately 10% water until a random distribution of fibers by visual examination was achieved. In this step, 10% moisture content was considered for the prevention of segregation of fibers from the soil. Second, a certain amount of water was then added to the mixture of fibers and soil prepared in the first step to achieve the optimum moisture content. On the other hand, three steps were involved in the mixing of mixture of soil, fiber, and lime. The first step was thoroughly mixing lime with soil with approximately 10% water. The following two steps were as those for the preparation of the mixture of soil and fiber. After the completion of the static compaction, all the samples were transferred into a curing room of 25 ± 1 °C and 95% humidity in which they were cured for 21 days.

2.3. Triaxial Testing Procedure

Conventional undrained triaxial tests were conducted on unconsolidated samples using a strain-controlled apparatus as per ASTM D2850–15 [63]. For each of the four kinds of sample, samples were tested at four different confining pressures of 100, 200, 300, and 400 kPa at a strain rate of 0.8 mm/min. During the loading process and continuing through to the post-failure regime, deviatoric stress was recorded as a function of axial strain. The maximum axial strain reached in a triaxial test was determined by the sample failure mode. If the sample failed in a strain-hardening mode, the maximum axial strain was 20%; otherwise, it was slightly greater than the axial strain at which the peak deviatoric stress was observed. The sample deformation was measured by using a dial indicator attached to the testing apparatus. The measured sample deformation was normalized by the height of the sample, which gave the axial strain of the sample. All of the samples were cured for 28 days before testing.

3. Results and Discussion

The results derived from the UU triaxial tests are presented and compared in terms of stress–strain relation, shear strength parameters, secant modulus in the early loading process, and failure pattern. During these comparisons, the coupling effect of wheat straw fiber reinforcement and lime stabilization is discussed in regard to magnitude. The microstructural mechanisms of the coupling effect are interpreted using the results of SEM analysis.

3.1. Stress–Strain Relation

Deviatoric stress–axial strain relations for untreated soil, lime-stabilized soil, fiber-reinforced soil, and fiber-reinforced soil stabilized with lime are shown in Figure 2. Note that the deviatoric stress–axial strain relations for treated soil are discussed for only one confining pressure (i.e., 200 kPa) due to

the similarity of the stress–strain behavior between different confining pressures. It can be seen that untreated soil and fiber-reinforced soil exhibit strain-hardening behavior while strain-softening occurs in lime-stabilized soil and fiber-reinforced soil stabilized with lime. The strain-softening behavior of fiber-reinforced soil stabilized with lime is not as severe as that of lime-stabilized soil comparing Figure 2b with Figure 2d, indicating that the addition of wheat straw fibers into lime-stabilized soil contributes to the change of the stress–strain behavior of lime-stabilized Hefei clayey soil from strain-softening to a more ductile one. The magnitude of this contribution varies depending on fiber content at a constant lime content and seems to increase with increasing fiber content from 0.2% to 0.4% and then decrease slightly when further increasing the fiber content. Therefore, the optimum fiber content for the fully mobilized fiber to improve the strain-softening behavior of the lime-stabilized soil is approximately 0.4%. The shear strength of the tested samples also displays the difference in the effects of fiber reinforcement, lime stabilization, and a combination of them. The effect of fiber reinforcement on the shear strength is of benefit subjected to the control of an upper bound. The upper bound is an increase of 133.7 kPa in the shear strength achieved by the addition of 0.4% fibers. A higher amount of fibers tends to induce segregation and tangling of fibers which jeopardizes the effective interaction of fibers and soil particles. Lime stabilization enormously increases the shear strength of Hefei clayey soil. When the lime contents were 2%, 4%, and 6%, the shear strengths of the samples were 243.2, 307.8, and 226.2 kPa, respectively. The increases in shear strength brought by lime stabilization are almost 2 times that derived from fiber reinforcement. A combination of 0.4% fiber reinforcement and 4% lime stabilization produces a 322.2 kPa strength increase compared to the shear strength of untreated soil, which is smaller than the sum of strength increase brought by 0.4% fiber reinforcement (133.7 kPa) and the strength increase caused by 4% lime stabilization (307.8 kPa). This difference in strength increase indicates that the combined effect of fiber reinforcement and lime stabilization is not a simple summation of their respective effects. Therefore, the effect of fiber reinforcement and that of lime stabilization are coupled. This coupling effect can be accounted for through SEM analysis.

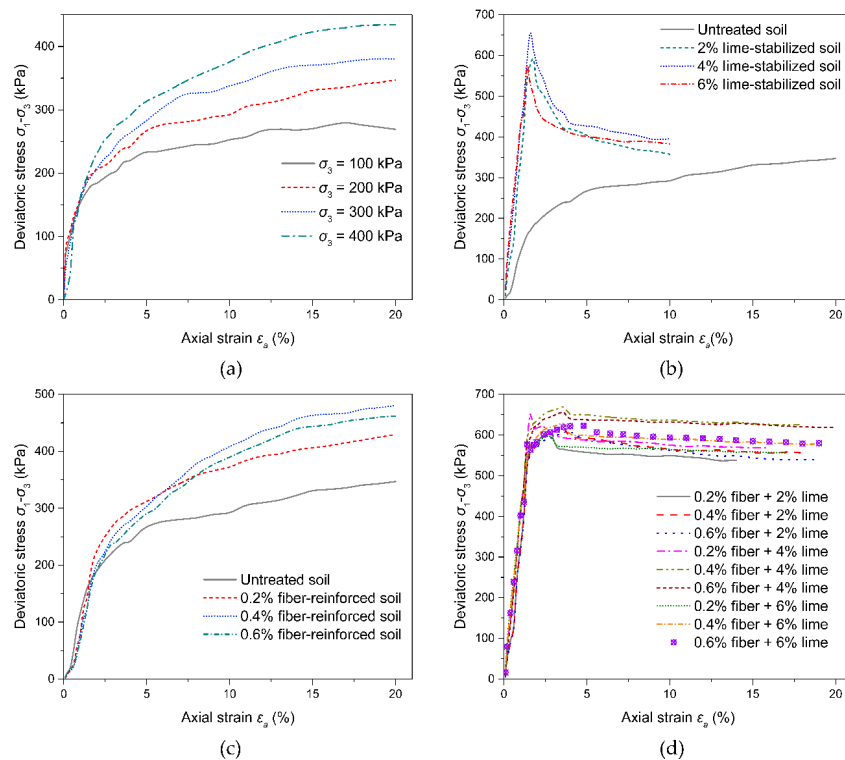


Figure 2. Stress–strain relations for untreated soil tested at various confining pressures and treated soil tested at 200 kPa: (a) untreated soil, (b) lime-stabilized soil, (c) fiber-reinforced soil, and (d) fiber-reinforced soil stabilized with lime.

3.2. Shear Strength Parameters

The shear strength parameters (i.e., cohesion and angle of internal friction) of the treated soil varied depending on the type and content of additives. Figure 3 shows a comparison of the shear strength parameters at different contents of wheat straw fiber and lime. It is shown that until reaching a fiber content of 0.4%, both the cohesion and the angle of internal friction increased nonlinearly with increasing fiber content. After that, a slight reduction was observed. The maximum cohesion of the fiber-reinforced soil, achieved at a fiber content of 0.4%, was 1.13 times the cohesion of untreated soil. That value for the angle of internal friction was 1.17. When lime was introduced to soil samples reinforced with 0.4% fiber, the maximum cohesions and angles of internal friction increased observably. The maximum cohesions were, respectively, 1.18, 1.28, and 1.16 times that of untreated soil for lime contents of 2%, 4%, and 6%. These values for the maximum angles of internal friction were, respectively, 1.27, 1.26, and 1.30. In addition, it was indicated that the effect of lime content on cohesion was slightly different to that on the angle of internal friction. At a fixed fiber content, the cohesion decreased with a further increase in lime content above 4%. However, the angle of internal friction increased with increasing lime content from 4% to 6%. Generally, a combination of fiber reinforcement and lime stabilization led to shear strength parameters much greater than those achieved when fiber and lime were used separately.

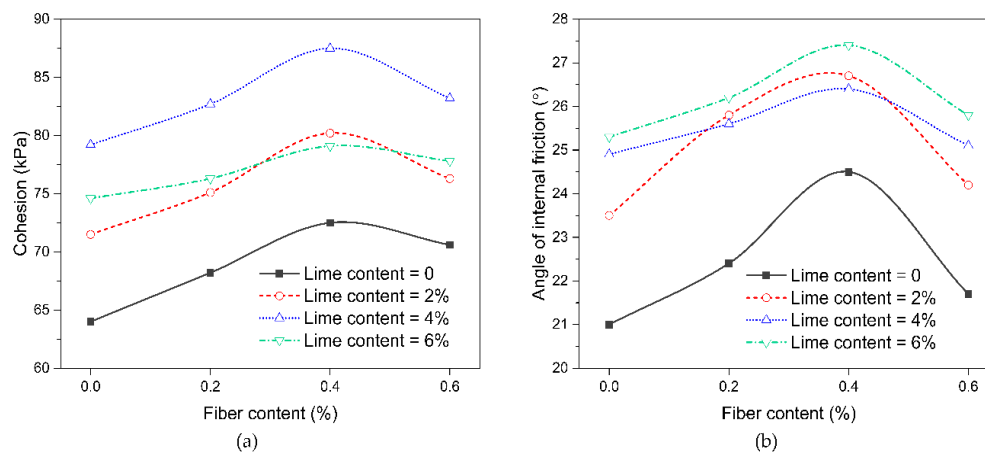


Figure 3. Shear strength parameters for soil samples with additives of different contents: (a) cohesion and (b) angle of internal friction.

3.3. Secant Modulus

The secant modulus is defined as the ratio of the deviatoric stress to the corresponding axial strain at a particular point on the stress–strain curve. Based on this definition, the secant moduli of untreated soil, fiber-reinforced soil, lime-stabilized soil, and fiber-reinforced soil stabilized with lime were calculated at four small strain levels. The variations in these moduli with strain level are shown in Figure 4. In this figure, the characteristics of the variations vary from case to case. For fiber-reinforced soil and fiber-reinforced soil stabilized with 2% lime, the secant moduli increase with increasing strain level. For fiber-reinforced soil stabilized with 6% lime, an increase in strain level leads to a reduction in the secant moduli. However, no consistent trend is observed for either lime-stabilized soil or fiber-reinforced soil stabilized with 4% lime. The varied characteristics of the variations in these moduli can hardly be explained using the experimental evidence collected in this study, showing the need to conduct more relevant laboratory work.

The secant moduli at a 1.2% axial strain level for untreated soil, fiber-reinforced soil, lime-stabilized soil, and fiber-reinforced soil stabilized with lime are shown in parallel in Figure 5, where the percentages represent the rates of increase in the secant moduli compared to that of untreated soil. Note that each of the percentages presented below the bars was calculated by adding

the rate of increase in the secant modulus produced by fiber reinforcement to that produced by lime stabilization. From this figure, it is indicated that lime stabilization can increase the secant modulus of Hefei clayey soil at a 1.2% axial strain level. The increase in the secant modulus reaches a maximum of 249.2% at 4% lime content. On the other hand, the secant modulus is reduced by fiber reinforcement. The reduction in the secant modulus increases with increasing fiber content. At 0.6% fiber content, the reduction reaches 31.3%.

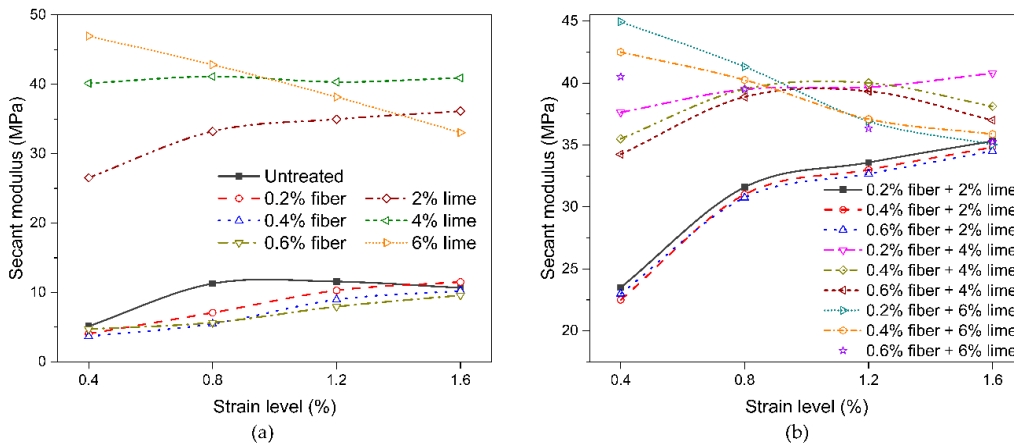


Figure 4. Secant moduli at four strain levels tested at $\sigma_3 = 200$ kPa: (a) samples reinforced with fibers or stabilized with lime and (b) fiber-reinforced samples stabilized with lime.

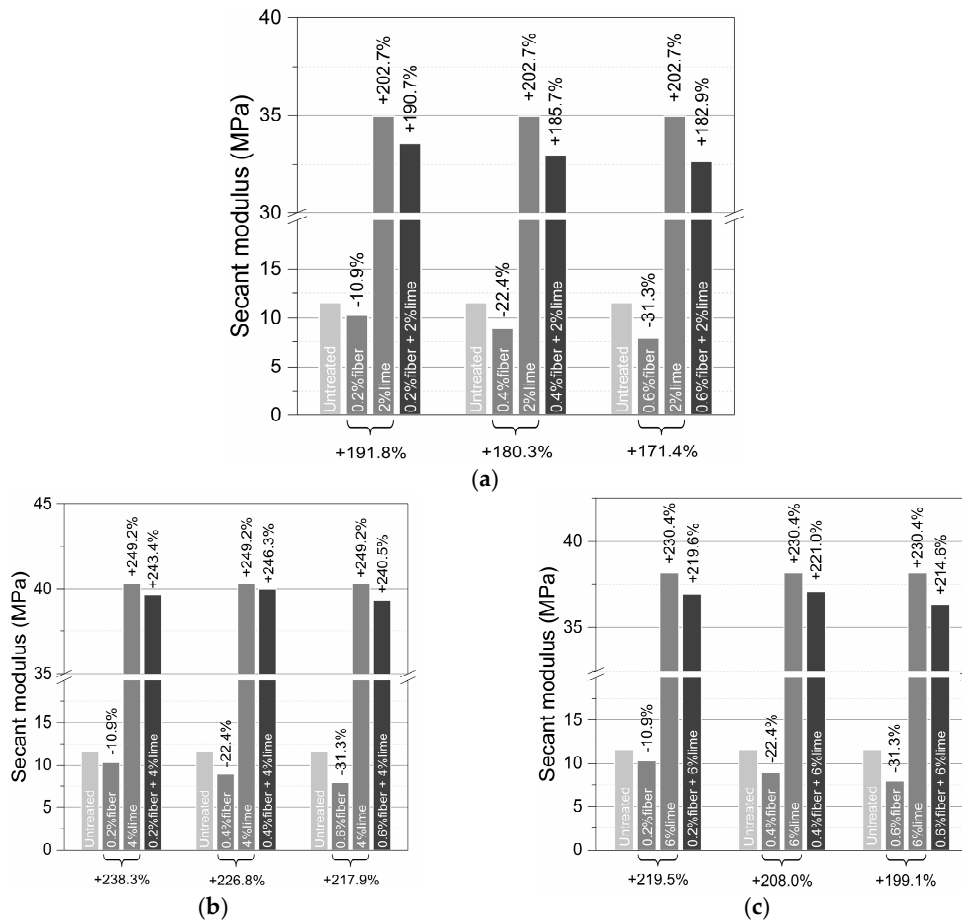


Figure 5. Secant moduli at a 1.2% strain level tested at $\sigma_3 = 200$ kPa: (a) 2% lime content, (b) 4% lime content, and (c) 6% lime content. The percentages represent the rates of increase in the secant moduli compared to the untreated one.

Despite the fact that fiber reinforcement reduces the soil's secant modulus, a combination of fiber reinforcement and lime stabilization greatly increases the secant modulus. This increase in the secant modulus decreases with increasing fiber content when the lime content is kept constant. Meanwhile, keeping a constant fiber content, the increase in the secant modulus due to a combination of fiber reinforcement and lime stabilization reaches its maximum at a lime content of 4%. Besides this, the increase in the secant modulus due to a combination of fiber reinforcement and lime stabilization is greater than the summation of the respective increases in the secant modulus produced by fiber reinforcement and lime stabilization for all of the considered cases except for 0.2% fiber-reinforced soil stabilized with 2% lime. Therefore, the coupling effect of fiber reinforcement and lime stabilization on the secant modulus of the soil at a 1.2% strain level is that the presence of fibers improves the ability of lime to increase the soil's secant modulus.

3.4. Failure Pattern

The failure patterns of samples after the completion of the triaxial tests are compared in Figure 6 for untreated soil, fiber-reinforced soil, lime-stabilized soil, and fiber-reinforced soil stabilized with lime. The comparison shows that the failures of untreated soil and fiber-reinforced soil hold a similar pattern where no noticeable shear band is observed. This failure pattern is known as plastic failure and is consistent with the observed strain-hardening behavior shown in Figure 2a,c. In spite of this similar failure pattern, a slightly smaller lateral deformation of the sample can be noticed for fiber-reinforced soil compared to that of untreated soil. The difference in sample lateral deformation is attributable to the presence of wheat straw fibers in which the induced tensile stress will restrain the lateral swelling of Hefei clayey soil.

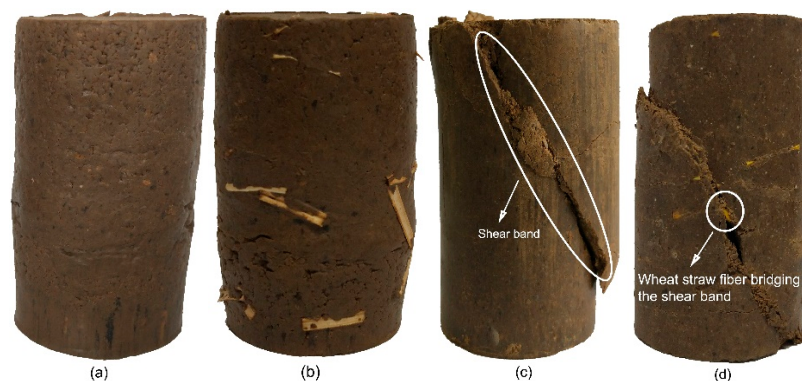


Figure 6. Photographs of sample failure patterns (at a 20% axial strain level) in triaxial compression tested at $\sigma_3 = 200$ kPa: (a) untreated soil, (b) 0.4% fiber-reinforced soil, (c) 4% lime-stabilized soil, and (d) 0.4% fiber-reinforced soil stabilized with 4% lime.

A greatly different failure pattern from the plastic failure pattern discussed above characterizes the failures of lime-stabilized soil and fiber-reinforced soil stabilized with lime, as indicated in Figure 6c,d. Characteristic of this failure pattern is the appearance of a dominant shear failure band oriented at an angle from the horizontal greater than $\pi/4$ throughout the samples. Besides this, within this failure pattern, brittleness is involved, which can be referred to as an effect of the strain-softening behavior observed in Figure 2b,d. Comparison between the shear failure bands which developed in lime-stabilized soil and in fiber-reinforced soil stabilized with lime indicates that the fibers bridging the shear failure band in the fiber-reinforced soil stabilized with lime (as shown in Figure 6d) can restrain the development of the shear failure band and thus contribute to more ductile stress–strain behavior compared to that of lime-stabilized soil.

3.5. Microstructural Mechanisms of the Coupling Effect

The coupling effect of wheat straw fiber reinforcement and lime stabilization on the stress–strain relation, shear strength parameters, secant modulus, and failure pattern of treated Hefei clayey soil has its explanation in microstructural mechanisms which can be captured through SEM analysis. SEM micrographs showing the honeycomb pattern of wheat straw fibers are shown in Figure 7. Figure 8 shows the SEM micrographs for lime, wheat straw fiber surface wrinkles due to friction, untreated soil, fiber surface morphologies in fiber-reinforced soil and fiber-reinforced soil stabilized with lime, and soil particle morphology in lime-stabilized soil. It can be observed from Figure 8b that the mobilization of the fiber reinforcing effect is driven by friction developed during physical contact between soil particles and the fiber surface. This physical contact can be also inferred from the experimental evidence presented in Figure 9.

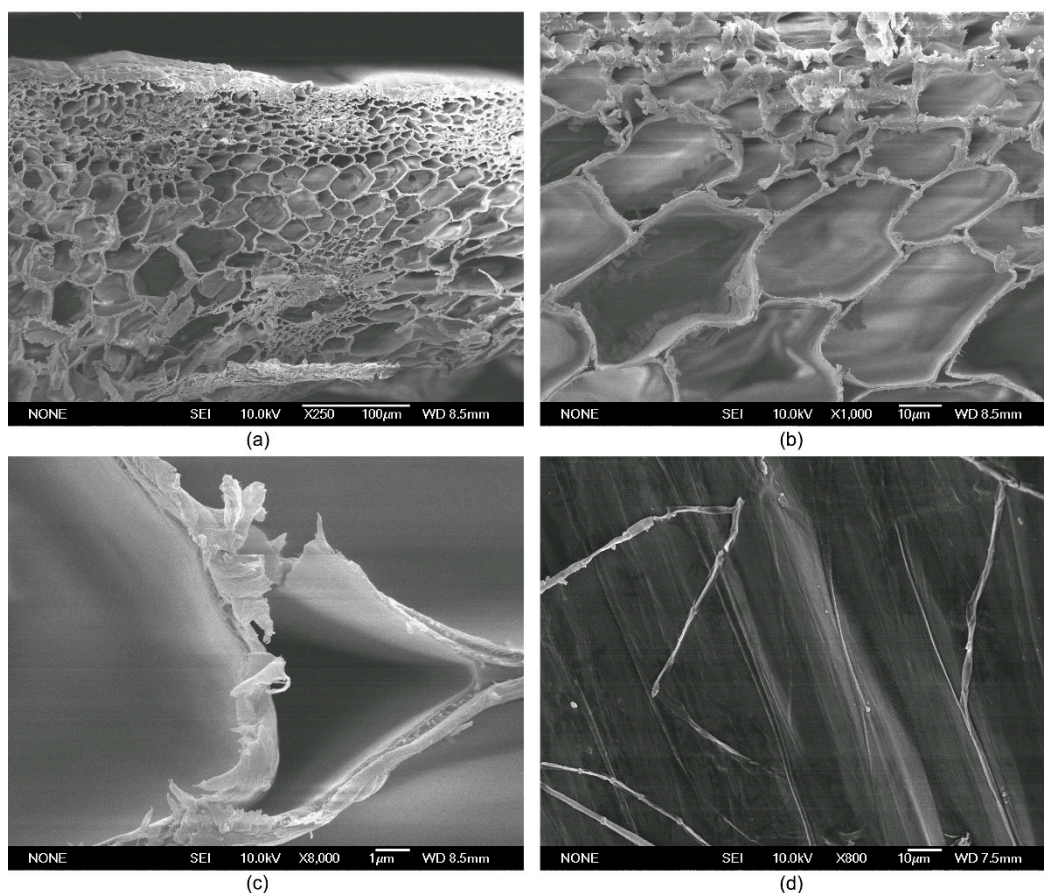


Figure 7. SEM micrographs of the wheat straw fiber’s honeycomb pattern ((a) magnification of 250×; (b) magnification of 1000×; and (c) magnification of 8000×) and the wheat straw fiber surface ((d) magnification of 800×).

The mechanism of stabilizing soil with lime is tripartite. First, the water within the soil reacts with the added lime, which reduces the soil moisture content and thus speeds up the soil consolidation process. Second, the sandification effect due to the addition of lime causes hydrophobic behavior in the soil particles, which can restrain the formation of soil particle packets and densify the soil fabric. Third, the chemical reaction of lime and soil produces a vast number of cementitious gels which fill most of the distributed pores and bind soil particles together (as shown in Figure 10), creating a denser soil fabric. The soil fabric improved by lime through these three ways is reflected in the final soil particle morphology shown in Figure 8e.

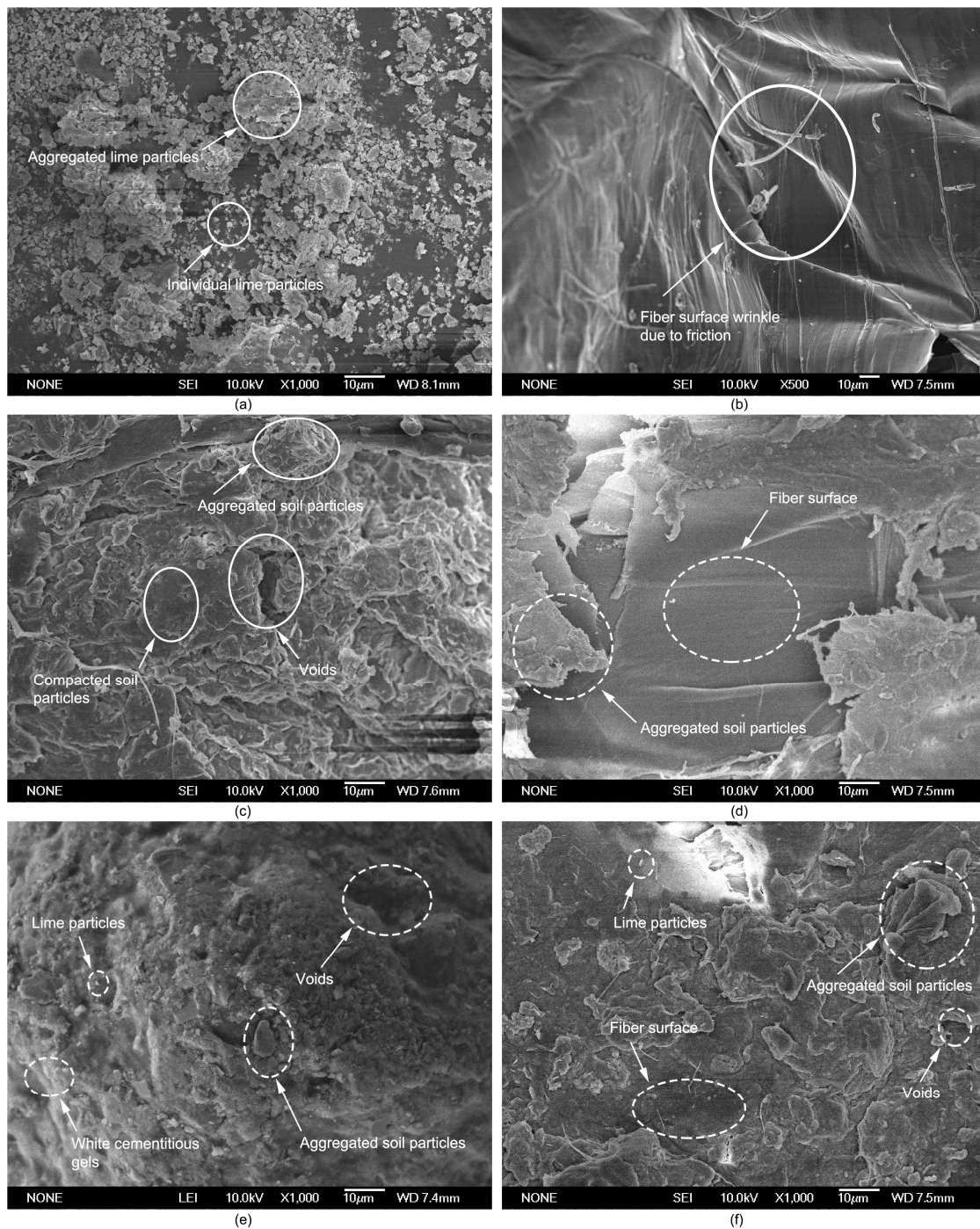


Figure 8. SEM micrographs showing (a) lime; (b) a fiber surface wrinkle; (c) untreated soil; (d) the fiber surface morphology in 0.4% fiber-reinforced soil; (e) the soil particle morphology in 4% lime-stabilized soil; and (f) the fiber surface morphology in 0.4% fiber-reinforced soil stabilized with 4% lime.

The simultaneous existence of fiber and lime within a sample of fiber-reinforced soil stabilized with lime creates a more effective fiber reinforcing effect and faster lime stabilization development than when they exist alone. Because of the water channels offered by the surfaces and honeycomb pattern (as shown in Figure 7) of wheat straw fibers, the process of the chemical reaction between lime and water becomes faster, causing a higher secant modulus than when lime exists alone. On the other hand, more effective contact between fibers and soil particles for fiber-reinforced soil stabilized with lime can

be noticed in the comparison between fiber surface morphologies presented in Figure 8d,f. The reason for this is that the three ways by which lime stabilization functions contribute to denser soil fabric and a smaller volume of soil particle packets. Besides this, the coverage of cementitious gels produced by the presence of lime on wheat straw fiber surfaces can improve the physical interaction between fibers and soil particles because of the increased friction coefficient caused by the high surface roughness and rigidity of these cementitious gels.

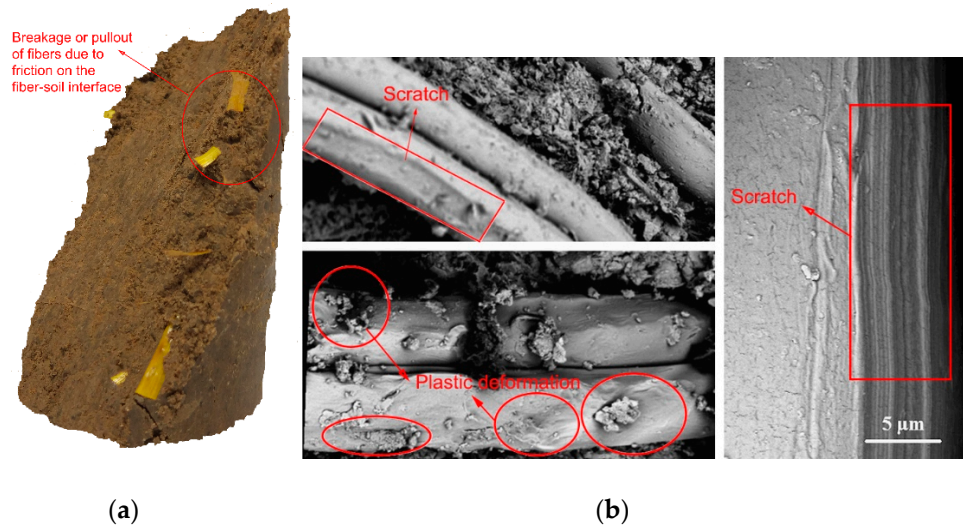


Figure 9. Experimental evidence of friction between fiber and soil showing (a) breakage or pullout of fibers and (b) a scratch formed on the fiber surface (modified from Tang et al. (2007) [64] and Tang et al. (2010) [65]).

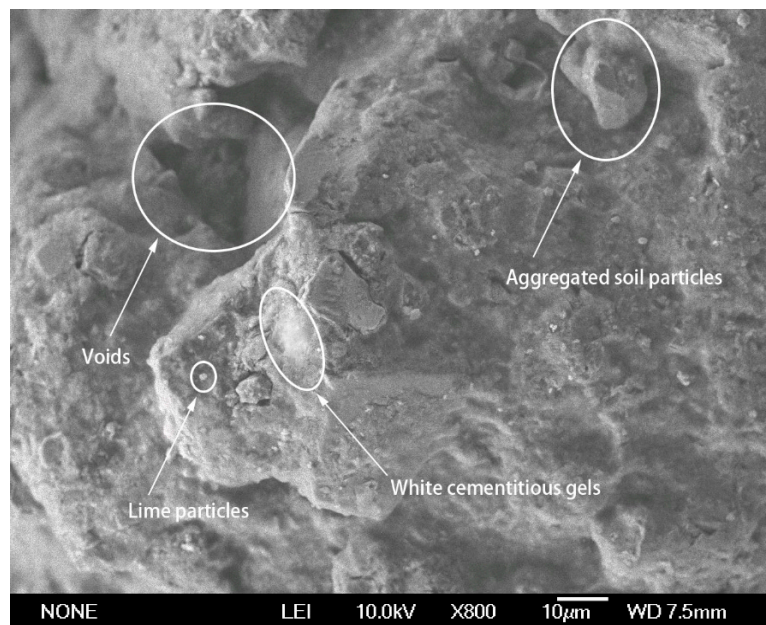


Figure 10. SEM micrograph showing white cementitious gels produced by the chemical reaction of soil and lime.

4. Conclusions

Conventional triaxial tests and SEM analysis were conducted to study the coupling effect of wheat straw fiber reinforcement and lime stabilization on the behavior of Hefei clayey soil. Quantitative estimation of the coupling effect was performed using comparisons of the induced results by fiber

reinforcement, lime stabilization, and a combination of them in terms of the stress–strain relation, secant modulus, and failure pattern. The microstructural mechanisms involved in the coupling effect were analyzed with the help of SEM micrographs. The following conclusions were drawn.

(1) The strain-hardening behavior of Hefei clayey soil was retained by wheat straw fiber reinforcement but was changed to strain-softening when the soil was stabilized with lime or treated with a combination of fiber reinforcement and lime stabilization. The addition of even a small amount of wheat straw fiber improved greatly the strain-softening of soil stabilized with lime alone.

(2) A combination of fiber reinforcement and lime stabilization produced a larger increase in the secant modulus at a 1.2% strain level than did only stabilizing soil with lime at an identical lime content despite the fact that reinforcing soil using only fibers could reduce its secant modulus.

(3) The addition of fibers into lime-stabilized soil restrained the development of a shear band. The restraint was attributable to the tensile stress induced in the fibers bridging the shear band and was beneficial to the occurrence of brittle failure at a greater strain level compared to the case where only lime was incorporated.

(4) The microstructural mechanisms by which the coupling effect of fiber reinforcement and lime stabilization occurs were found to be the development of the chemical reaction between soil and lime being quickened by the water channels offered by wheat straw fibers and that the effective physical interaction between fibers and soil particles was strengthened by the dense soil fabric and the cementitious gels created by lime stabilization.

(5) The shear strength parameters were observably increased by combining wheat straw fiber reinforcement and lime stabilization. The maximum cohesion and angle of internal friction were, respectively, 1.37 and 1.30 times those of untreated soil. With increasing lime content, an asymptotic increase in the cohesion existed, but this was not the case for the angle of internal friction.

Author Contributions: Y.W. proposed the idea of combining wheat straw fiber reinforcement with lime stabilization for improving the behavior of Hefei clayey soil. P.G. prepared the manuscript. X.L. performed the triaxial compression tests. H.L. performed the SEM tests. Y.L. discussed the test results. H.Y. revised the manuscript.

Funding: This research work was funded by the National Natural Science Foundation of China (51774107), the Opening Project of State Key Laboratory of Explosion Science and Technology, Beijing Institute of Technology (KFJJ19-02M), the Fundamental Research Funds for the Hefei Key Project Construction Administration (2013CGAZ0771), and the Fundamental Research Funds of the Housing and Construction Department of Anhui Province (2013YF-27).

Conflicts of Interest: The authors declare no conflict of interest.

References

1. Meng, J.; Cao, P.; Huang, J.; Lin, H.; Chen, Y.; Cao, R. Second-order cone programming formulation of discontinuous deformation analysis. *Int. J. Numer. Methods Eng.* **2019**. [[CrossRef](#)]
2. Lin, H.; Wang, H.; Fan, X.; Cao, P.; Zhou, K. Particle size distribution effects on deformation properties of graded aggregate base under cyclic loading. *Eur. J. Environ. Civ. Eng.* **2018**. [[CrossRef](#)]
3. Wang, D.; Wang, H.; Di, S. Mechanical properties and microstructure of magnesia-fly ash pastes. *Road Mater. Pavement Des.* **2019**. [[CrossRef](#)]
4. Chen, Y.F.; Lin, H. Consistency analysis of Hoek-Brown and equivalent Mohr-coulomb parameters in calculating slope safety factor. *Bull. Eng. Geol. Environ.* **2018**, *1–3*. [[CrossRef](#)]
5. Wang, H.; Lin, H. Non-linear shear strength criterion for a rock joint with consideration of friction variation. *Geotech. Geol. Eng.* **2018**, *36*, 3731–3741. [[CrossRef](#)]
6. Cao, R.; Cao, P.; Lin, H.; Fan, X.; Zhang, C.; Liu, T. Crack Initiation, Propagation, and Failure Characteristics of Jointed Rock or Rock-Like Specimens: A Review. *Adv. Civ. Eng.* **2019**, *2019*, 6975751. [[CrossRef](#)]
7. Lin, H.; Xiong, W.; Yan, Q. Modified Formula for the Tensile Strength as Obtained by the Flattened Brazilian Disk Test. *Rock Mech. Rock Eng.* **2016**, *49*, 579–1586. [[CrossRef](#)]

8. Zhao, Y.L.; Wang, Y.X.; Wang, W.; Tang, L.; Liu, Q.; Cheng, G. Modeling of rheological fracture behavior of rock cracks subjected to hydraulic pressure and far field stresses. *Theor. Appl. Fract. Mech.* **2019**, *101*, 59–66. [[CrossRef](#)]
9. Wang, H.; Nie, W.; Cheng, W.M.; Liu, Q.; Jin, H. Effects of air volume ratio parameters on air curtain dust suppression in a rock tunnel's fully-mechanized working face. *Adv. Powder Technol.* **2018**, *29*, 230–244. [[CrossRef](#)]
10. Liu, Q.; Nie, W.; Hua, Y.; Peng, H.; Liu, C.; Wei, C. Research on tunnel ventilation systems: Dust diffusion and pollution behaviour by air curtains based on CFD technology and field measurement. *Build. Environ.* **2019**, *147*, 444–460. [[CrossRef](#)]
11. Yang, S.B.; Nie, W.; Lv, S.S.; Liu, Z.Q.; Peng, H.T.; Ma, X.; Cai, P.C.; Xu, W. Effects of spraying pressure and installation angle of nozzles on atomization characteristics of external spraying system at a fully-mechanized mining face. *Powder Technol.* **2019**, *343*, 754–764. [[CrossRef](#)]
12. Cai, P.; Nie, W.; Chen, D.W.; Yang, S.B.; Liu, Z.Q. Effect of air flowrate on pollutant dispersion pattern of coal dust particles at fully mechanized mining face based on numerical simulation. *Fuel* **2019**, *239*, 623–635. [[CrossRef](#)]
13. Bao, Q.; Nie, W.; Liu, C.; Liu, Y.; Zhang, H.; Wang, H.; Jin, H. Preparation and Characterization of a Binary-Graft-Based, Water-Absorbing Dust Suppressant for Coal Transportation. *J. Appl. Polym. Sci.* **2019**, *136*. [[CrossRef](#)]
14. Jin, H.; Nie, W.; Zhang, H.; Liu, Y.; Bao, Q.; Wang, H.; Huang, D. Preparation and characterization of a novel environmentally friendly coal dust suppressant. *J. Appl. Polym. Sci.* **2019**, *136*. [[CrossRef](#)]
15. Peng, H.; Nie, W.; Cai, P. Development of a novel wind-assisted centralized spraying dedusting device for dust suppression in a fully mechanized mining face. *Environ. Sci. Pollut. Res.* **2018**, *26*, 3292–3307. [[CrossRef](#)] [[PubMed](#)]
16. Nie, W.; Wei, W.L.; Cai, P.; Liu, Z.; Liu, Q.; Ma, H.; Liu, H. Simulation experiments on the controllability of dust diffusion by means of multi-radial vortex airflow. *Adv. Powder Technol.* **2018**, *29*, 835–847. [[CrossRef](#)]
17. Zhang, C.Y.; Pu, C.Z.; Cao, R.H.; Jiang, T.T.; Huang, G. The stability and roof-support optimization of roadways passing through unfavorable geological bodies using advanced detection and monitoring methods, among others, in the Sanmenxia Bauxite Mine in China's Henan Province. *Bull. Eng. Geol. Environ.* **2019**, 1–13. [[CrossRef](#)]
18. Wang, Y.X.; Shan, S.B.; Zhang, C.S.; Guo, P.P. Seismic response of tunnel lining structure in a thick expansive soil stratum. *Tunn. Undergr. Space Technol.* **2019**, in press.
19. Cao, R.H.; Cao, P.; Lin, H.; Ma, G.; Chen, Y. Failure characteristics of intermittent fissures under a compressive-shear test: Experimental and numerical analyses. *Theor. Appl. Fract. Mech.* **2018**, *96*, 740–757. [[CrossRef](#)]
20. Mooney, M.A.; Rinehart, R.V. Field monitoring of roller vibration during compaction of subgrade soil. *J. Geotech. Geoenviron. Eng.* **2007**, *133*. [[CrossRef](#)]
21. Wu, F.; Chen, J.; Zou, Q.L. A nonlinear creep damage model for salt rock. *Int. J. Damage Mech.* **2018**. [[CrossRef](#)]
22. Fan, X.; Li, K.; Lai, H.; Xie, Y.; Cao, R.; Zheng, J. Internal stress distribution and cracking around flaws and openings of rock block under uniaxial compression: A particle mechanics approach. *Comput. Geotech.* **2018**, *102*, 28–38. [[CrossRef](#)]
23. Basha, E.A.; Hashim, R.; Mahmud, H.B.; Muntohar, A.S. Stabilization of residual soil with rice husk ash and cement. *Constr. Build. Mater.* **2005**, *19*, 448–453. [[CrossRef](#)]
24. Wang, Y.X.; Guo, P.P.; Lin, H.; Li, X.; Zhao, Y.L.; Yuan, B.X.; Liu, Y.; Cao, P. Numerical Analysis of Fiber-Reinforced Soils based on the Equivalent Additional Stress Concept. *Int. J. Geomech.* **2019**, in press.
25. Wang, Y.X.; Lin, H.; Zhao, Y.L.; Li, X.; Guo, P.P.; Liu, Y. Analysis of fracturing characteristics of unconfined rock plate under edge on impact loading. *Eur. J. Environ. Civ. Eng.* **2019**. [[CrossRef](#)]
26. Chen, R.; Ge, Y.H.; Chen, Z.K.; Liu, J.; Zhao, Y.R.; Li, Z.H. Analytical solution for one-dimensional contaminant diffusion through unsaturated soils beneath geomembrane. *J. Hydrol.* **2019**, *568*, 260–274. [[CrossRef](#)]
27. Chen, R.; Huang, J.W.; Chen, Z.K.; Xu, Y.; Liu, J.; Ge, Y.H. Effect of root density of wheat and okra on hydraulic properties of an unsaturated compacted loam. *Eur. J. Soil Sci.* **2019**. [[CrossRef](#)]

28. Yetimoglu, T.; Salbas, O. A study on shear strength of sands reinforced with randomly distributed discrete fibers. *Geotext. Geomembr.* **2003**, *21*, 103–110. [[CrossRef](#)]
29. Wang, Y.; Guo, P.; Shan, S.; Yuan, H.; Yuan, B. Study on strength influence mechanism of fiber-reinforced expansive soil using jute. *Geotech. Geol. Eng.* **2016**, *34*, 1079–1088. [[CrossRef](#)]
30. Tang, C.S.; Wang, D.Y.; Cui, Y.J.; Shi, B. Tensile strength of fiber-reinforced soil. *J. Mater. Civ. Eng.* **2016**, *28*. [[CrossRef](#)]
31. Wang, Y.; Guo, P.; Dai, F.; Li, X.; Zhao, Y.; Liu, Y. Behavior and modeling of fiber-reinforced clay under triaxial compression by combining the superposition method with the energy-based homogenization technique. *Int. J. Geomech.* **2018**, *18*. [[CrossRef](#)]
32. Viswanadham, B.V.S.; Phanikumar, B.R.; Mukherjee, R.V. Swelling behaviour of a geofiber-reinforced expansive soil. *Geotext. Geomembr.* **2009**, *27*, 73–76. [[CrossRef](#)]
33. Wang, D.; Du, Y.; Xiao, J. Shear properties of stabilized loess using novel reactive magnesia-bearing binders. *J. Mater. Civ. Eng.* **2019**, *31*. [[CrossRef](#)]
34. Zhao, Y.L.; Tang, J.Z.; Chen, Y.; Zhang, L.Y.; Wang, W.J.; Liao, J.P. Hydromechanical coupling tests for mechanical and permeability characteristics of fractured limestone in complete stress–strain process. *Environ. Earth Sci.* **2017**, *76*. [[CrossRef](#)]
35. Park, S.S. Unconfined compressive strength and ductility of fiber-reinforced cemented sand. *Constr. Build. Mater.* **2011**, *25*, 1134–1138. [[CrossRef](#)]
36. Wang, Y.-X.; Guo, P.-P.; Ren, W.-X.; Yuan, B.-X.; Yuan, H.-P.; Zhao, Y.-L.; Shan, S.-B.; Cao, P. Laboratory investigation on strength characteristics of expansive soil treated with jute fiber reinforcement. *Int. J. Geomech.* **2017**, *17*. [[CrossRef](#)]
37. Zhao, Y.L.; Luo, S.L.; Wang, Y.X.; Wang, W.J.; Zhang, L.Y.; Wan, W. Numerical analysis of karst water inrush and a criterion for establishing the width of water-resistant rock pillars. *Mine Water Environ.* **2017**, *36*, 508–519. [[CrossRef](#)]
38. Michalowski, R.L.; Čermák, J. Triaxial compression of sand reinforced with fibers. *J. Geotech. Geoenviron. Eng.* **2003**, *129*. [[CrossRef](#)]
39. Bell, F.G. Lime stabilization of clay minerals and soils. *Eng. Geol.* **1996**, *42*, 223–237. [[CrossRef](#)]
40. Narasimha Rao, S.; Rajasekaran, G. Reaction products formed in lime-stabilized marine Clays. *J. Geotech. Eng.* **1996**, *122*. [[CrossRef](#)]
41. Rajasekaran, G.; Narasimha Rao, S. Compressibility behaviour of lime-treated marine clay. *Ocean Eng.* **2002**, *29*, 545–559. [[CrossRef](#)]
42. Wang, D.; Zentar, R.; Abriak, N.E. Durability and swelling of solidified/stabilized dredged marine soils with class F fly ash, cement and lime. *J. Mater. Civ. Eng.* **2018**, *30*. [[CrossRef](#)]
43. Wang, D.; Zentar, R.; Abriak, N.E.; Di, S.J. Long-term mechanical performance of marine sediments solidified with cement, lime and fly ash. *Mar. Georesourcesgeotechnol.* **2018**, *36*, 123–130. [[CrossRef](#)]
44. Al-Rawas, A.A.; Hago, A.W.; Al-Sarmi, H. Effect of lime, cement and Sarooj (artificial pozzolan) on the swelling potential of an expansive soil from Oman. *Build. Environ.* **2005**, *40*, 681–687. [[CrossRef](#)]
45. Lu, M.M.; Li, D.X.; Jing, H.W.; Deng, Y.B. Analytical solution for consolidation of band-shaped drain based on an equivalent annular drain. *Int. J. Geomech.* **2019**. [[CrossRef](#)]
46. Ninov, J.; Donchev, I. Lime stabilization of clay from the ‘Mirkovo’ depositPart, I. Kinetics and mechanism of the processes. *J. Therm. Anal. Calorim.* **2008**, *91*, 487–490. [[CrossRef](#)]
47. Yuan, B.; Sun, M.; Wang, Y.; Zhai, L.; Luo, Q.; Zhang, X. A full 3D displacement measuring system for 3D displacement field of soil around a laterally loaded pile in transparent soil. *Int. J. Geomech.* **2019**, *19*. [[CrossRef](#)]
48. Fan, X.; Lin, H.; Lai, H.P.; Cao, R.H.; Liu, J. Numerical analysis of the compressive and shear failure behavior of rock containing multi-intermittent joints. *C. R. Mécanique* **2019**, *347*, 33–48. [[CrossRef](#)]
49. Cai, Y.; Shi, B.; Ng, C.W.W.; Tang, C.S. Effect of polypropylene fibre and lime admixture on engineering properties of clayey soil. *Eng. Geol.* **2016**, *87*, 230–240. [[CrossRef](#)]
50. Anggraini, V.; Asadi, A.; Farzadnia, N.; Jahangirian, H.; Huat, B.B.K. Reinforcement benefits of nanomodified coir fiber in lime-treated marine clay. *J. Mater. Civ. Eng.* **2016**, *28*. [[CrossRef](#)]
51. Kumar, A.; Walia, B.S.; Bajaj, A. Influence of fly ash, lime, and polyester fibers on compaction and strength properties of expansive soil. *J. Mater. Civ. Eng.* **2007**, *19*. [[CrossRef](#)]

52. He, S.; Li, J. Modeling nonlinear elastic behavior of reinforced soil using artificial neural networks. *Appl. Soft Comput.* **2009**, *9*, 954–961. [[CrossRef](#)]
53. Anggraini, V.; Asadi, A.; Huat, B.B.K.; Nahazanan, H. Effects of coir fibers on tensile and compressive strength of lime treated soft soil. *Measurement* **2015**, *59*, 372–381. [[CrossRef](#)]
54. Yuan, B.; Xu, K.; Wang, Y.; Chen, R.; Luo, Q. Investigation of deflection of a laterally loaded pile and soil deformation using the PIV technique. *Int. J. Geomech.* **2017**, *17*. [[CrossRef](#)]
55. Zhao, Y.L.; Wang, Y.X.; Wang, W.J.; Wan, W.; Tang, J.Z. Modeling of non-linear rheological behavior of hard rock using triaxial rheological experiment. *Int. J. Rock Mech. Min. Sci.* **2017**, *93*, 66–75. [[CrossRef](#)]
56. Lu, M.M.; Jing, H.W.; Zhou, A.N.; Xie, K.H. Analytical models for consolidation of combined composite ground improved by impervious columns and vertical drains. *Int. J. Numer. Anal. Methods Geomech.* **2018**, *42*, 871–888. [[CrossRef](#)]
57. Qu, J.; Sun, Z. Strength behavior of Shanghai clayey soil reinforced with wheat straw fibers. *Geotech. Geol. Eng.* **2016**, *34*, 515–527. [[CrossRef](#)]
58. Li, M.; Chai, S.X.; Zhang, H.Y.; Du, H.P.; Wei, L. Feasibility of saline soil reinforced with treated wheat straw and lime. *Soils Found.* **2012**, *52*, 228–238. [[CrossRef](#)]
59. Wang, D.; Wang, H.; Jiang, Y. Water immersion-induced strength performance of solidified soils with reactive MgO—A green and low carbon binder. *J. Test. Eval.* **2019**. [[CrossRef](#)]
60. Zhao, Y.L.; Zhang, L.Y.; Wang, W.J.; Wan, W.; Li, S.Q.; Ma, W.H.; Wang, Y.X. Creep behavior of intact and cracked limestone under multi-level loading and unloading cycles. *Rock Mech. Rock Eng.* **2017**, *50*, 1409–1424. [[CrossRef](#)]
61. Lu, M.M.; Scott, W.S.; Buddhima, I.; Jing, H.W.; Xie, K.H. A new analytical model for consolidation with multiple vertical drains. *Int. J. Numer. Anal. Methods Geomech.* **2016**, *40*, 1623–1640. [[CrossRef](#)]
62. Lu, M.M.; Jing, H.W.; Zhou, Y.; Xie, K.H. General analytical model for consolidation of stone columns-reinforced ground and combined composite ground. *Int. J. Geomech.* **2017**, *17*. [[CrossRef](#)]
63. ASTM. *Standard Test Method for Unconsolidated-Undrained Triaxial Compression Test on Cohesive Soils*; ASTM International: West Conshohocken, PA, USA, 2015.
64. Tang, C.-S.; Shi, B.; Zhao, L.-Z. Interfacial shear strength of fiber reinforced soil. *Geotext. Geomembr.* **2010**, *28*, 54–62. [[CrossRef](#)]
65. Tang, C.; Shi, B.; Gao, W.; Chen, F.; Cai, Y. Strength and mechanical behavior of short polypropylene fiber reinforced and cement stabilized clayey soil. *Geotext. Geomembr.* **2007**, *25*, 194–202. [[CrossRef](#)]



© 2019 by the authors. Licensee MDPI, Basel, Switzerland. This article is an open access article distributed under the terms and conditions of the Creative Commons Attribution (CC BY) license (<http://creativecommons.org/licenses/by/4.0/>).